MIMO Radar Waveform Design With Constant Modulus and Similarity Constraints

Guolong Cui, *Member, IEEE*, Hongbin Li, *Senior Member, IEEE*, and Muralidhar Rangaswamy, *Fellow, IEEE*

***Abstract*—We consider the problem of waveform design for Multiple-Input Multiple-Output (MIMO) radar in the presence of signal-dependent interference embedded in white Gaussian disturbance. We present two sequential optimization procedures to maximize the Signal to Interference plus Noise Ratio (SINR), accounting for a constant modulus constraint as well as a similarity constraint involving a known radar waveform with some desired properties (e.g., in terms of pulse compression and ambiguity). The presented sequential optimization algorithms, based on a relaxation method, yield solutions with good accuracy. Their computational complexity is linear in the number of iterations and trials in the randomized procedure and polynomial in the receive filter length. Finally, we evaluate the proposed techniques, by considering their SINR performance, beam pattern as well as pulse compression property, via numerical simulations.**

***Index Terms*—Constant modulus and similarity constraints, MIMO radar, sequential optimization algorithms, waveform design.**

I. Introduction

MULTIPLE-INPUT Multiple-Output (MIMO) radar, unlike a standard phased-array radar emitting scaled versions of a single waveform, transmits multiple probing signals, which provides extra degrees of freedom in the design of the radar system as well as in developing more sophisticated signal processing algorithms [1]. According to the configuration of the antennas, the MIMO radar systems can be classified into two types. The first one [2], [3] employs widely separated transmit and receive antennas such that a target can be viewed from different spatial aspects, resulting in spatial diversity of the system. The spatial diversity can improve the performance of detection and angle estimation. The second one [4], [5] involves transmit and receive antennas that are colocated (spaced close enough). By exploiting waveform diversity, MIMO radar with colocated antennas can improve the interference rejection capability, parameter identifiability, and provide the flexibility for transmit beam pattern design.

The problem of waveform design for MIMO radar has received considerable attention recently. These works can be classified into two categories. The first category addresses the waveform design problem by considering only the radar transmitter. Specific issues that have been considered in this category include the transmit beam pattern design and radar ambiguity function design. The purpose of the transmit beam pattern design is to control the emitted power distribution in the spatial domain through the covariance matrix of the waveforms. In [6], the covariance matrix was devised to achieve or approximate a desired spatial beam pattern; also introduced there was a method to synthesize constant modulus waveforms for a given covariance matrix. In [7], the waveform covariance matrix was designed to attain a desired beam pattern as well as to minimize the cross-correlation between the probing signals at a number of given target locations. In [8], the authors considered constant modulus signal design to approximate a desired beam pattern while minimizing the levels of both the autocorrelation and cross-correlation sidelobes at given spatial angles. Meanwhile, ambiguity function design was considered in [9], [10] to improve the radar performance in the spatial, range, and Doppler domains by optimizing the entire waveforms instead of their covariances.

The second category approaches the waveform design problem by jointly optimizing the radar transmitter and receiver. In the absence of signal-dependent interferences (e.g., clutter), in [11], the maximization of the detection probability was studied to design the optimum code matrix; the mutual information between the received waveforms and the target radar signatures was employed to design the transmit waveform for extended target [12], [13]. Other information theoretic based transmit waveform designs were considered in [14] for multiple extended targets. In [15], transmit waveforms were optimized for multiple targets in the presence of spatially colored interference and noise, based on several design criteria, including minimizing the trace, determinant, and the largest eigenvalue of the Cramér-Rao Bound (CRB) matrix. In the presence of signal-dependent interferences, MIMO waveform design was examined by maximizing the Signal to Interference plus Noise Ratio (SINR) given knowledge of the target and interferences, using a gradient based algorithm; in addition, suboptimal solutions were provided when partial information of the target or interferences is known [16]. The framework was employed for adaptive waveform design based on training data [17]. Using

Manuscript received May 12, 2013; revised August 28, 2013; accepted October 18, 2013. Date of publication October 30, 2013; date of current version December 24, 2013. The associate editor coordinating the review of this manuscript and approving it for publication was Prof. Ljubisa Stankovic. The work of M. Rangaswamy was supported by the Air Force Office of Scientific Research under project 13RY10COR.

G. Cui was with the Department of Electrical and Computer Engineering, Stevens Institute of Technology, Hoboken, NJ 07030 USA. He is now with the School of Electronic Engineering, University of Electronic Science and Technology of China, Chengdu, China (e-mail: guolongcui@gmail.com; cuiguolong@uestc.edu.cn).

H. Li is with the Department of Electrical and Computer Engineering, Stevens Institute of Technology, Hoboken, NJ 07030 USA (e-mail: hongbin.li@stevens.edu).

M. Rangaswamy is with the RF Exploitation Branch, Air Force Research Laboratory (AFRL)/RYAP, WPAFB, OH 45433 USA (e-mail: Muralidhar.Rangaswamy@wpafb.af.mil).

Color versions of one or more of the figures in this paper are available online at http://ieeexplore.ieee.org.

Digital Object Identifier 10.1109/TSP.2013.2288086

1053-587X © 2013 IEEE. Personal use is permitted, but republication/redistribution requires IEEE permission.
See http://www.ieee.org/publications_standards/publications/rights/index.html for more information.

the same SINR criterion, a different iterative algorithm, based on a cyclic optimization of the waveform and the receive filter, was proposed in [18], which guarantees nondecreasing SINR performance with each additional iteration. In [19], MIMO waveform was devised by minimizing the estimation error of the Minimum Mean Squared Error (MMSE) estimators for uncorrelated and correlated targets.

In practical applications, several design constraints, such as the constant modulus constraint [8], the similarity constraint [20], [21], and the Peak-to-Average Ratio (PAR) constraint [22], are often considered in waveform design. The constant modulus or PAR constraint is needed because radar amplifiers usually work in a saturation condition, which prohibits amplitude modulation in radar waveforms. Meanwhile, a similarity constraint uses a known waveform as a benchmark, which allows the designed waveform to share some of the good ambiguity properties of the known waveform. However, most of the prior studies on waveform design only considered an energy constraint. Limited studies belonging to the aforementioned first category of work (e.g., [8], [18]) incorporated the constant modulus design constraint. For the second category of design in the presence of signal-dependent interferences, MIMO radar waveform design accounting with the general constraints (i.e., constant modulus, PAR, and similarity constraints) appears not available in the open literature.

In this paper, we investigate the MIMO radar waveform design in the presence of signal-dependent interference and white Gaussian noise, by taking into account the constant modulus constraint as well as a similarity constraint between the designed signal and a known radar waveform. More specifically, we consider a narrow band colocated MIMO radar involving point like targets in the presence of signal-dependent interferences. Using the SINR design criterion, we formulate the optimization problem that consists of a non-convex objective function of the transmit waveform and non-convex sets of the constraints [23]. We propose two constrained sequential optimization algorithms to maximize the SINR by jointly optimizing the transmit signal and receive filter. At each iteration of the first algorithm, the receive filter is designed using the Minimum Variance Distortionless Response (MVDR) method [24] to suppress the interferences, and then the transmit waveform is obtained by maximizing the SINR subject to a constant modulus and a similarity constraints. As to the second algorithm, the transmit and receive filters can jointly process interference suppression. Hence, in some situations where the target and interference are close to each other, the second algorithm may perform better than the first one as shown in our simulation. Each iteration of both algorithms involves an NP-hard optimization problem, we employ a relaxation and randomization approach which is known to yield approximate solutions with good accuracy [21], [25]–[27]. The resulting computational complexity is linear in the number of iterations as well as the number of trials in the randomized procedure, and polynomial in the receive filter length. The proposed techniques are evaluated by computer simulation, in terms of their SINR behaviors, beam pattern as well as pulse compression property.

The rest of the paper is organized as follows. In Section II, we introduce the signal model involving both the transmitted and received signals in a colocated MIMO radar. In Section III, we discuss the waveform design criterion. In Section IV, we present two constrained sequential optimization algorithms. In Section V, we evaluate the proposed algorithms as well as unconstrained waveform design algorithms by computer simulations. Finally, in Section VI, we provide concluding remarks and possible future research tracks.

II. MIMO Signal Model

Consider a colocated narrow band MIMO radar system with N_T transmit antennas and N_R receive antennas, where each transmit element emits a different waveform $s_m(n)$, $m = 1, \ldots, N_T$, $n = 1, \ldots, N$, through omnidirectional transmission, with N being the number of samples of each transmitted pulse. Let $\boldsymbol{s}(n)$ be an $N_T \times 1$ vector collecting the nth sample of the N_T waveforms. Then, the signal seen at a location with angle θ is given by

$$\boldsymbol{a}_t^T(\theta)\boldsymbol{s}(n),\ n = 1, \ldots, N, \tag{1}$$

where $\boldsymbol{a}_t(\theta)$ denotes the $N_T \times 1$ transmit steering vector containing complex-valued elements, and $(\cdot)^T$ denotes the transpose. As an example, for a uniform linear array (ULA) with half-wavelength separation between two adjacent array elements, the steering vector is given by [5]

$$\boldsymbol{a}_t(\theta) = \frac{1}{\sqrt{N_T}}\left[1, e^{-j\pi\sin\theta}, \ldots, e^{-j\pi(N_T-1)\sin\theta}\right]^T. \tag{2}$$

Suppose there is a target located at angle θ_0 along with K signal-dependent interference sources located at $\theta_k \neq \theta_0$, $k = 1, \ldots, K$. The baseband equivalent of the signals at the receive array are given by [28]

$$\boldsymbol{x}(n) = \alpha_0\boldsymbol{a}_r(\theta_0)\boldsymbol{a}_t^T(\theta_0)\boldsymbol{s}(n) + \sum_{k=1}^{K}\alpha_k\boldsymbol{a}_r(\theta_k)\boldsymbol{a}_t^T(\theta_k)\boldsymbol{s}(n) + \boldsymbol{v}(n), \tag{3}$$

where α_0 and α_k denote respectively the complex amplitudes of the target and the kth interference source and $\boldsymbol{a}_r(\theta)$ is the $N_R \times 1$ propagation vector due to the propagation delays from a source to the receive elements. Similarly, for a ULA with half-wavelength spaced element,

$$\boldsymbol{a}_r(\theta) = \frac{1}{\sqrt{N_R}}\left[1, e^{-j\pi\sin\theta}, \ldots, e^{-j\pi(N_R-1)\sin\theta}\right]^T. \tag{4}$$

Finally, $\boldsymbol{v}(n)$ in (3) is an $N_R \times 1$ circular complex white Gaussian noise vector with zero mean and covariance matrix $\sigma_v^2\mathbf{I}$.

Let $\boldsymbol{x} = [\boldsymbol{x}^T(1), \ldots, \boldsymbol{x}^T(N)]^T$, $\boldsymbol{s} = [\boldsymbol{s}^T(1), \ldots, \boldsymbol{s}^T(N)]^T$, and $\boldsymbol{v} = [\boldsymbol{v}^T(1), \ldots, \boldsymbol{v}^T(N)]^T$. Then, (3) can be recast as

$$\boldsymbol{x} = \alpha_0\mathbf{A}(\theta_0)\boldsymbol{s} + \sum_{k=1}^{K}\alpha_k\mathbf{A}(\theta_k)\boldsymbol{s} + \boldsymbol{v}, \tag{5}$$

where $\mathbf{A}(\theta)$ is determined by the look angle θ, given by

$$\mathbf{A}(\theta) = \mathbf{I}_N \otimes \left[\boldsymbol{a}_r(\theta)\boldsymbol{a}_t^T(\theta)\right], \tag{6}$$

while $\otimes$ denotes the Kronecker product.

III. MIMO Radar Waveform Design Criterion

This section is devoted to mathematical formulation the optimization waveform design criterion, namely, maximizing the output SINR criterion subject to some additional constraints.

A. Output SINR

The detection probability of a target is usually a monotonically increasing function of the SINR for the case of Gaussian interference. As a consequence, we examine waveform design for MIMO radars by maximizing the output SINR. Specifically, a linear Finite Impulse Response (FIR) receive filter $\boldsymbol{w}$, which is a $N_R N \times 1$ vector with complex-valued components, is used for SINR maximization. The output of the filter can be written as

$$r = \boldsymbol{w}^\dagger \boldsymbol{x} = \alpha_0 \boldsymbol{w}^\dagger \mathbf{A}(\theta_0)\boldsymbol{s} + \boldsymbol{w}^\dagger \sum_{k=1}^{K} \alpha_k \mathbf{A}(\theta_k)\boldsymbol{s} + \boldsymbol{w}^\dagger \boldsymbol{v}, \quad (7)$$

where $(\cdot)^\dagger$ denotes the transpose conjugate. The output SINR $\rho(\boldsymbol{s}, \boldsymbol{w})$ can be expressed as

$$\begin{aligned}\rho(\boldsymbol{s}, \boldsymbol{w}) &= \frac{E[|\alpha_0 \boldsymbol{w}^\dagger \mathbf{A}(\theta_0)\boldsymbol{s}|^2]}{E[|\boldsymbol{w}^\dagger \sum_{k=1}^{K} \alpha_k \mathbf{A}(\theta_k)\boldsymbol{s}|^2] + \sigma_n^2 \boldsymbol{w}^\dagger \boldsymbol{w}} \\ &= \frac{\mathrm{SNR}|\boldsymbol{w}^\dagger \mathbf{A}(\theta_0)\boldsymbol{s}|^2}{\boldsymbol{w}^\dagger \boldsymbol{\Sigma}_I(\boldsymbol{s})\boldsymbol{w} + \boldsymbol{w}^\dagger \boldsymbol{w}},\end{aligned} \quad (8)$$

where $E[\cdot]$ denotes the statistical expectation, $\boldsymbol{\Sigma}_I(\boldsymbol{s})$ is

$$\boldsymbol{\Sigma}_I(\boldsymbol{s}) = \sum_{k=1}^{K} \mathrm{INR}_k \mathbf{A}(\theta_k)\boldsymbol{s}\boldsymbol{s}^\dagger \mathbf{A}^\dagger(\theta_k), \quad (9)$$

and $\mathrm{SNR} = E[|\alpha_0|^2]/\sigma_v^2$ denotes the Signal-to-Noise Ratio (SNR), and $\mathrm{INR}_k = E[|\alpha_k|^2]/\sigma_v^2$ is the kth Interference-to-Noise Ratio (INR).

Some remarks are now in order. First, the clutter energy $\boldsymbol{w}^\dagger \boldsymbol{\Sigma}_I(\boldsymbol{s})\boldsymbol{w}$ functionally depends on the receive filter $\boldsymbol{w}$ and the transmit waveform $\boldsymbol{s}$ through $\boldsymbol{\Sigma}_I(\boldsymbol{s})$. Second, the objective function requires knowledge of the angles of the interferences θ_k for $k = 1, \ldots, K$. In practice, the exact locations of the interferences might be unknown. If the locations of the interferences can be modeled as random variables, we assume that the mean of these random variables are known, in which case θ_k represent the *mean locations* of the interferences. In Section V, we consider cases when the exact locations and, respectively, mean locations of the interferences are known, and numerically examine the impact on the proposed techniques.

Our purpose is to design the transmit waveform $\boldsymbol{s}$ and receive filter $\boldsymbol{w}$ by maximizing the output SINR $\rho(\boldsymbol{s}, \boldsymbol{w})$ (8). It should be noted that the max-SINR approach was employed for waveform design in the presence of signal-dependent interferences before, but only under an energy constraint of the waveform $\boldsymbol{s}$ (i.e., $\|\boldsymbol{s}\|^2 = 1$ where $\|\cdot\|$ denotes the Euclidean norm) in [16], [18], which resulted in waveforms that are not constant modulus. However, in practical applications, constant modulus waveforms are often required due to the limit of nonlinear radar amplifiers. Moreover, as noted in [16], [18], the resulting waveforms generally do not exhibit good pulse compression and ambiguity function properties. Therefore, additional constraints are necessary in the waveform design problem. Here, we focus on the constant modulus and similarity constraints.

B. Constant Modulus and Similarity Constraints

Constant modulus constraint is to enforce the modulus of each element of the waveform $\boldsymbol{s}$ to be a constant. Specifically, considering the normalized transmitted energy (i.e., $\|\boldsymbol{s}\|^2 = 1$), the element of $\boldsymbol{s}$ can be expressed as

$$\boldsymbol{s}(k) = \frac{1}{\sqrt{N_T N}} e^{j\varphi_k}, \ k = 1, \ldots, N_T N, \quad (10)$$

where φ_k denotes the phase of each element of the waveform $\boldsymbol{s}$, which is to be determined in the waveform design problem.

Enforcing a *similarity constraint* on the waveform $\boldsymbol{s}$ allows a tradeoff between optimizing the output SINR and controlling other desired waveform properties (i.e., pulse compression and ambiguity) [21]. This is equivalent to optimizing the detection performance in a suitable neighborhood of a reference waveform which is known to have good properties. We assume that $\boldsymbol{s}_0$ is the reference waveform, and consider the following similarity constraint:

$$\|\boldsymbol{s} - \boldsymbol{s}_0\|_\infty \le \epsilon, \quad (11)$$

where $\|\boldsymbol{x}\|_\infty = \max\{x_1, \ldots, x_{N_T N}\}$ denotes the infinity norm and ϵ is a real parameter ruling the extent of the similarity. The constraint (11) is equivalent to

$$|\boldsymbol{s}(k) - \boldsymbol{s}_0(k)| \le \epsilon, \ k = 1, \ldots, N_T N. \quad (12)$$

Finally, accounting for the constant modulus constraint, (12) can be further recast as [21]

$$\varphi_k = \arg \boldsymbol{s}(k) \in [\gamma_k, \gamma_k + \delta_k], \ k = 1, \ldots, N_T N, \quad (13)$$

where γ_k and δ_k are respectively given by

$$\gamma_k = \arg \boldsymbol{s}_0(k) - \arccos(1 - \epsilon^2/2), \quad (14)$$

$$\delta_k = 2\arccos(1 - \epsilon^2/2), \quad (15)$$

with $0 \le \epsilon \le 2$. Notice that for $\epsilon = 0$, the waveform $\boldsymbol{s}$ is identical to the reference waveform $\boldsymbol{s}_0$, whereas the similarity constraint vanishes and only the constant modulus constraint is in effect when $\epsilon = 2$.

IV. Proposed Sequential Optimization Algorithms

Based on the aforementioned discussions, the waveform design can be formulated in terms of the following constrained optimization problem

$$\begin{aligned}\max_{\boldsymbol{s},\boldsymbol{w}} \quad & \rho(\boldsymbol{s}, \boldsymbol{w}) = \frac{\mathrm{SNR}|\boldsymbol{w}^\dagger \mathbf{A}(\theta_0)\boldsymbol{s}|^2}{\boldsymbol{w}^\dagger \boldsymbol{\Sigma}_I(\boldsymbol{s})\boldsymbol{w} + \boldsymbol{w}^\dagger \boldsymbol{w}}, \\ \text{s.t.} \quad & \arg \boldsymbol{s}(k) \in [\gamma_k, \gamma_k + \delta_k], \\ & |\boldsymbol{s}(k)| = 1/\sqrt{N_T N}, k = 1, \ldots, N_T N.\end{aligned} \quad (16)$$

Generally speaking, there is no closed-form solution to the problem (16). In the following, we provide two sequential optimization algorithms to solve the problem.

A. Sequential Optimization Algorithm 1

An inspection of the problem (16) reveals that it does not have any constraint on $\boldsymbol{w}$. Thus, we can first optimize $\rho(\boldsymbol{s}, \boldsymbol{w})$ with respect to $\boldsymbol{w}$ in terms of $\boldsymbol{s}$, then solve it with respect to $\boldsymbol{s}$, and so

on and so forth in an iterative fashion. Specifically, with a given $\boldsymbol{s}$, the optimization problem (16) with respect to $\boldsymbol{w}$ is equivalent to

$$\max_{\boldsymbol{w}} \frac{|\boldsymbol{w}^\dagger \mathbf{A}(\theta_0)\boldsymbol{s}|^2}{\boldsymbol{w}^\dagger \boldsymbol{\Sigma}_I(\boldsymbol{s})\boldsymbol{w} + \boldsymbol{w}^\dagger \boldsymbol{w}}. \tag{17}$$

It is easy to see that the problem (17) is equivalent to the well-known MVDR problem [24]

$$\begin{aligned} \min_{\boldsymbol{w}} \quad & \boldsymbol{w}^\dagger \left[\boldsymbol{\Sigma}_I(\boldsymbol{s}) + \mathbf{I}\right] \boldsymbol{w} \\ \text{s.t.} \quad & \boldsymbol{w}^\dagger \mathbf{A}(\theta_0)\boldsymbol{s} = 1. \end{aligned} \tag{18}$$

The solution is given by

$$\boldsymbol{w} = \frac{[\boldsymbol{\Sigma}_I(\boldsymbol{s}) + \mathbf{I}]^{-1}\mathbf{A}(\theta_0)\boldsymbol{s}}{\boldsymbol{s}^\dagger \mathbf{A}^\dagger(\theta_0)[\boldsymbol{\Sigma}_I(\boldsymbol{s}) + \mathbf{I}]^{-1}\mathbf{A}(\theta_0)\boldsymbol{s}}. \tag{19}$$

Substituting (19) into (16), and after some algebraic manipulations, the problem reduces to

$$\begin{aligned} \max_{\boldsymbol{s}} \quad & \boldsymbol{s}^\dagger \boldsymbol{\Phi}(\boldsymbol{s})\boldsymbol{s}, \\ \text{s.t.} \quad & \arg \boldsymbol{s}(k) \in [\gamma_k, \gamma_k + \delta_k] \\ & |\boldsymbol{s}(k)| = 1/\sqrt{N_T N}, k = 1, \ldots, N_T N, \end{aligned} \tag{20}$$

where $\boldsymbol{\Phi}(\boldsymbol{s})$ is

$$\boldsymbol{\Phi}(\boldsymbol{s}) = \mathbf{A}^\dagger(\theta_0)[\boldsymbol{\Sigma}_I(\boldsymbol{s}) + \mathbf{I}]^{-1}\mathbf{A}(\theta_0). \tag{21}$$

Inspecting on (20), some remarks are in order. First, the upper bound of the SINR is available when $\boldsymbol{\Sigma}_I(\boldsymbol{s}) = 0$, i.e., there is no interference. Thus, the following inequality holds

$$\max_{\boldsymbol{s},\boldsymbol{w}} \rho(\boldsymbol{s}, \boldsymbol{w}) \leq \mathrm{SINR}_{UB}, \tag{22}$$

where $\mathrm{SINR}_{UB} = \mathrm{SNR}\, \lambda_{max}\left(\mathbf{A}^\dagger(\theta_0)\mathbf{A}(\theta_0)\right)$ denotes the upper bound of SINR, and $\lambda_{max}(\cdot)$ denotes the maximum eigenvalue of the matrix.

If we ignore the dependence of $\boldsymbol{\Phi}(\boldsymbol{s})$ on the waveforms, i.e., $\boldsymbol{\Phi}(\boldsymbol{s}) = \boldsymbol{\Phi}_0$, where $\boldsymbol{\Phi}_0$ denotes a constant matrix, then (20) reduces to the problem in [21]. In other words, [21] considered only phase code design with *signal-independent* interferences. In the following, we briefly explain the Semi-Definite Relaxation (SDR) and randomization method [25], which were used in [21] to solve their phase code design problem. These methods will be extended and applied iteratively in our sequential algorithm for MIMO waveform design with *signal-dependent* interferences.

Specifically, when $\boldsymbol{\Phi}(\boldsymbol{s}) = \boldsymbol{\Phi}_0$, we first relax the problem (20) to a Semi-Definite Programming (SDP) problem by dropping the similarity constraint and rank-one constraint [21]:

$$\begin{aligned} \max_{\mathbf{Z}} \quad & \mathrm{tr}\left(\boldsymbol{\Phi}_0 \mathbf{Z}\right), \\ \text{s.t.} \quad & \mathrm{diag}(\mathbf{Z}) = \mathbf{I}, \\ & \mathbf{Z} \succeq \mathbf{0}, \end{aligned} \tag{23}$$

where $\mathbf{Z} \succeq 0$ indicates that $\mathbf{Z}$ is a semi-definite matrix. The above SDP problem can be effective solved (e.g., by using the convex optimization toolbox CVX [23] in MATLAB). Then, we can use a randomization method [21], [25] to obtain an approximate solution of $\boldsymbol{s}$ from an SDR solution of (23). To illustrate the main idea, let $\boldsymbol{\xi}$ be a random vector with zero mean and covariance $\mathbf{Z} = E\{\boldsymbol{\xi}\boldsymbol{\xi}^\dagger\}$, and we consider the following stochastic optimization problem [25, eqn. (13)]:

$$\begin{aligned} \max_{\mathbf{Z}=E\{\boldsymbol{\xi}\boldsymbol{\xi}^\dagger\}\succeq \mathbf{0}} \quad & E\left\{\boldsymbol{\xi}^\dagger \boldsymbol{\Phi}_0 \boldsymbol{\xi}\right\}, \\ \text{s.t.} \quad & E\left\{\mathrm{diag}(\boldsymbol{\xi}\boldsymbol{\xi}^\dagger)\right\} = \mathbf{I}. \end{aligned} \tag{24}$$

One can see that the problem (24) is equivalent to the problem(23). Hence, the stochastic interpretation(24) of the SDR(23) allows us to obtain approximate rank-one solutions. Next, we describe how the randomization method can be integrated with the similarity constraint. Specifically, denote by $\mathbf{Z}_0^\star$ an optimal solution to (23), and generate independent identically distributed Gaussian random vectors $\boldsymbol{\xi}_i$, i.e., $\boldsymbol{\xi}_i \sim \mathcal{N}(\mathbf{0}, \mathbf{C}_0)$ for $i = 1, \ldots, L$, where L is the number of the randomization trials. The covariance matrix $\mathbf{C}_0$ is constructed as

$$\mathbf{C}_0 = \mathbf{Z}_0^\star \odot [\boldsymbol{p}_c \boldsymbol{p}_c^\dagger],$$

where $\odot$ denotes the Hadamard product, $\boldsymbol{p}_c$ is given by

$$\boldsymbol{p}_c = \frac{1}{\sqrt{N_T N}}[e^{-j\gamma_1}, \ldots, e^{-j\gamma_{N_T N}}]^T,$$

and γ_k is given in (14). Then, for the ith randomization trial, we assign

$$\boldsymbol{s}_i(k) = \boldsymbol{p}_c^*(k)\mu(\boldsymbol{\xi}_i(k)) \tag{25}$$

for $k = 1, \ldots, N_T N$, where

$$\mu(\boldsymbol{\xi}_i(k)) = \exp\left(j\frac{\arg(\boldsymbol{\xi}_i(k))}{2\pi}\delta_k\right),$$

and δ_k is given in (15). Since $0 \leq \frac{\arg(\boldsymbol{\xi}_i(k))}{2\pi} \leq 1$, it is clear that (25) ensures the similarity constraint (13) is met. Finally, the best solution among the L randomization is selected as the one which maximizes the objective function.

$$\boldsymbol{s}^\star = \arg\max_{\boldsymbol{s}_i} \boldsymbol{s}_i^\dagger \boldsymbol{\Phi}_0 \boldsymbol{s}_i.$$

The randomization method is known to yield to a good approximation provided that a solution for sufficient number of randomization trials is employed [21], [25].

However, with signal-dependent interference, matrix $\boldsymbol{\Phi}(\boldsymbol{s})$ as defined in (21) is a nonlinear function of the transmit waveform $\boldsymbol{s}$. As a result, the method in [21] cannot be directly used to our problem(20). In the following, we present a sequential optimization algorithm, which find the waveform $\boldsymbol{s}$ in an iterative fashion. Specifically, at the mth iteration, we first compute the matrix $\boldsymbol{\Phi}(\boldsymbol{s}_{m-1})$, where $\boldsymbol{s}_{m-1}$ denotes the waveform obtained from the $(m-1)$th iteration. Next, we solve $\boldsymbol{\Phi}(\boldsymbol{s}_{m-1})$ by using the relaxation and randomization method, and the solution $\boldsymbol{s}_{m-1}$ is used for the next-round iteration [21]; and then update $\boldsymbol{s}$. This process is repeated until the $\boldsymbol{\Phi}(\boldsymbol{s}_{m-1})$ improvement in the SINR becomes insignificant. We summarize this algorithm as follows.

Sequential Optimization Algorithm 1:

Input: $\{\theta_0, \theta_1, \ldots, \theta_K\}$, $\{\alpha_0, \alpha_1, \ldots, \alpha_K\}$, $\boldsymbol{s}_0$.
Output: A solution $\boldsymbol{s}^\star$ of (20).

1) For $m = 1$, initialize the transmit waveform $\boldsymbol{s}_1 = \boldsymbol{s}_0$.
2) Let $m = m + 1$, run the SDR and randomization method steps as follows.
   - Compute

$$\boldsymbol{\Phi}(\boldsymbol{s}_{m-1}) = \mathbf{A}^\dagger(\theta_0)(\boldsymbol{\Sigma}_I(\boldsymbol{s}_{m-1}) + \mathbf{I})^{-1}\mathbf{A}(\theta_0),$$
$$\boldsymbol{\Sigma}_I(\boldsymbol{s}_{m-1}) = \sum_{k=1}^{K} \mathrm{INR}_k \mathbf{A}(\theta_k)\boldsymbol{s}_{m-1}\boldsymbol{s}_{m-1}^\dagger \mathbf{A}^\dagger(\theta_k).$$

   The computational complexity involved in this step is in the order of $\mathcal{O}(N^3 N_T^3)$ floating point operations (flops) [29], where $\mathcal{O}(\cdot)$ denotes the Landau notation.
   - SDP: Solve the SDP problem below and denote by $\mathbf{Z}^\star$ a solution

$$\begin{aligned} (\mathrm{SDP})\ \max_{\mathbf{Z}} \quad & \mathrm{tr}\{\boldsymbol{\Phi}(\boldsymbol{s}_{m-1})\mathbf{Z}\}, \\ \text{s.t.} \quad & \mathrm{diag}(\mathbf{Z}) = \mathbf{I}, \\ & \mathbf{Z} \succeq 0, \end{aligned} \tag{26}$$

   which has the computational complexity of $\mathcal{O}(N^{3.5} N_T^{3.5})$ flops [26].
   - Randomization: Generate a random vector $\boldsymbol{\xi}_i \in C^{N_T N \times 1}$, $i = 1, \ldots, L$, where L is the number of randomization trials, from a circular complex Gaussian distribution with zero mean and covariance [21]

$$\mathbf{C} = \mathbf{Z}^\star \odot [\boldsymbol{p}_c \boldsymbol{p}_c^\dagger].$$

   For the ith randomization trial, let $\boldsymbol{s}_{m,i}(k) = \boldsymbol{p}_c^*(k)\mu(\boldsymbol{\xi}_i(k))$, $k = 1, \ldots, N_T N$, where

$$\mu(\boldsymbol{\xi}_i(k)) = \exp\left(j\frac{\arg(\boldsymbol{\xi}_i(k))}{2\pi}\delta_k\right).$$

   Choose $\boldsymbol{s}_m$ from $\boldsymbol{s}_{m,i}$, such that

$$\boldsymbol{s}_m = \arg\max_{\boldsymbol{s}_{m,i}} \boldsymbol{s}_{m,i}^\dagger \boldsymbol{\Phi}(\boldsymbol{s}_{m-1})\boldsymbol{s}_{m,i}.$$

   The computational complexity of this step for L randomization is in the order of $\mathcal{O}(LN^2 N_T^2)$ flops [26].
   - At the mth iteration, the modified object function in (20) can be calculated as

$$\rho_m = \boldsymbol{s}_m^\dagger \Phi(\boldsymbol{s}_{m-1})\boldsymbol{s}_m.$$

   If $|\rho_m - \rho_{m-1}| \le \varepsilon$, where ϵ is a user selected parameter to control convergence, output $\boldsymbol{s}^\star = \boldsymbol{s}_m$; otherwise, repeat step 2) until convergence.
   The computational complexity is in the order of $\mathcal{O}(N^2 N_T^2)$ flops [29].

Based on the computational analysis at each step, the overall computational complexity of Algorithm 1 for P iterations is in order of $\mathcal{O}(PN^{3.5}N_T^{3.5}) + \mathcal{O}(PLN^2 N_T^2)$, which mainly comes the SDP and randomization steps. Numerical simulations (see Section V) show that Algorithm 1 requires about $P \le 4$ iterations and $L \approx 20000$ randomization trials to converge a good solution. Nevertheless we cannot guarantee nondecreasing SINR with each iteration, since it is not the objective function of (20) but a modified one, i.e., $\boldsymbol{s}_m^\dagger \boldsymbol{\Phi}(\boldsymbol{s}_{m-1})\boldsymbol{s}_m$, that is optimized in each iteration. Furthermore, the number L of randomization required in each iteration (for each m) of Algorithm 1 is relatively large. Next, we present a different algorithm that ensures non-decreasing SINR with each iteration.

B. Sequential Optimization Algorithm 2

In this subsection, we introduce another sequential optimization procedure by iteratively optimizing the SINR with respect to the transmit waveform $\boldsymbol{s}$ and receive filter $\boldsymbol{w}$. Specifically, at the mth iteration, we first update the waveform to obtain $\boldsymbol{s}_m$ by maximizing the SINR with the receive filter fixed to the $\boldsymbol{w}_{m-1}$, which was obtained at the $(m-1)$th iteration; we then obtain an updated receive filter $\boldsymbol{w}_m$ by maximizing the SINR with the waveform fixed to $\boldsymbol{s}_m$. Repeat the procedure until the SINR convergence. A similar procedure was employed in [18], [26].

The optimization of $\boldsymbol{w}$ by maximizing the SINR for a given $\boldsymbol{s}$ has been obtained in (19). Now, we focus on the solution of $\boldsymbol{s}$ by maximizing the SINR for a given $\boldsymbol{w}$. To this end, the following proposition provides an alternative expression of SINR.

Proposition 4.1: An equivalent expression of the SINR defined in (8) is given by

$$\rho(\boldsymbol{s}, \boldsymbol{w}) = \frac{\mathrm{SNR}\left(\boldsymbol{s}^\dagger \boldsymbol{\Sigma}_t(\boldsymbol{w})\boldsymbol{s}\right)}{\boldsymbol{s}^\dagger \boldsymbol{\Sigma}_I(\boldsymbol{w})\boldsymbol{s} + \boldsymbol{w}^\dagger \boldsymbol{w}}, \tag{27}$$

where $\boldsymbol{\Sigma}_t(\boldsymbol{w})$ and $\boldsymbol{\Sigma}_I(\boldsymbol{w})$ are respectively

$$\boldsymbol{\Sigma}_t(\boldsymbol{w}) = \mathbf{A}^\dagger(\theta_0)\boldsymbol{w}\boldsymbol{w}^\dagger \mathbf{A}(\theta_0),$$
$$\boldsymbol{\Sigma}_I(\boldsymbol{w}) = \sum_{k=1}^{K} \mathrm{INR}_k \mathbf{A}^\dagger(\theta_k)\boldsymbol{w}\boldsymbol{w}^\dagger \mathbf{A}(\theta_k).$$

Proof: The expression (27) can be easily obtained by exploiting the following equalities in (8)

$$\begin{aligned} |\boldsymbol{w}^\dagger \mathbf{A}(\theta_0)\boldsymbol{s}|^2 &= |\boldsymbol{s}^\dagger \mathbf{A}^\dagger(\theta_0)\boldsymbol{w}|^2, \\ \left|\boldsymbol{w}^\dagger \sum_{k=1}^{K} \alpha_k \mathbf{A}(\theta_k)\boldsymbol{s}\right|^2 &= \left|\boldsymbol{s}^\dagger \sum_{k=1}^{K} \alpha_k^* \mathbf{A}^\dagger(\theta_k)\boldsymbol{w}\right|^2. \end{aligned} \tag{28}$$

■

Alternatively, being different from Algorithm 1, $\boldsymbol{s}$ can be obtained by optimizing the following problem for a fixed $\boldsymbol{w}$

$$\begin{aligned} \max_{\boldsymbol{s}} \quad & \frac{\boldsymbol{s}^\dagger \boldsymbol{\Sigma}_t(\boldsymbol{w})\boldsymbol{s}}{\boldsymbol{s}^\dagger \boldsymbol{\Sigma}_I(\boldsymbol{w})\boldsymbol{s} + \boldsymbol{w}^\dagger \boldsymbol{w}}, \\ \text{s.t.} \quad & \arg \boldsymbol{s}(k) \in [\gamma_k, \gamma_k + \delta_k] \\ & |\boldsymbol{s}(k)| = 1/\sqrt{N_T N}, k = 1, \ldots, N_T N. \end{aligned} \tag{29}$$

The problem (29) is non-convex optimization (the constraints define a non-convex set), and therefore an optimal solution is generally difficult to obtain. An approximate solution, based on the relaxation and randomization method, can be adopted. Specifically, we first relax the problem (29) to the following

fractional SDR problem, by dropping the similarity constraint and the rank-one constraint [26, eqn. 19]:

$$\begin{aligned} \max_{\mathbf{Z}} \quad & \frac{\mathrm{tr}(\mathbf{\Sigma}_t(\boldsymbol{w})\mathbf{Z})}{\mathrm{tr}(\mathbf{\Phi}(\boldsymbol{w})\mathbf{Z})} \\ \text{s.t.} \quad & \mathrm{diag}(\mathbf{Z}) = \mathbf{I} \\ & \mathbf{Z} \succeq 0, \end{aligned} \tag{30}$$

where $\mathbf{\Phi}(\boldsymbol{w}) = \mathbf{\Sigma}_I(\boldsymbol{w}) + \boldsymbol{w}^\dagger \boldsymbol{w}\mathbf{I}$. Let $\mathbf{X} = y\mathbf{Z}$, the fractional problem (30) is equivalent, via the Charnes-Cooper transformation, to an SDP problem [26, eqn. 20]:

$$\begin{aligned} \max_{\mathbf{X},y} \quad & \mathrm{tr}(\mathbf{\Sigma}_t(\boldsymbol{w})\mathbf{X}) \\ \text{s.t.} \quad & \mathrm{tr}(\mathbf{\Phi}(\boldsymbol{w})\mathbf{X}) = 1 \\ & \mathrm{diag}(\mathbf{X}) = y\mathbf{I} \\ & \mathbf{X} \succeq 0, y \geq 0. \end{aligned} \tag{31}$$

Suppose that $(\mathbf{X}^\star, y^\star)$ is a solution of (31). Then, $\mathbf{Z}^\star = \mathbf{X}^\star / y^\star$ is a solution of (30). Similar to Algorithm 1, randomization can be employed to restore the rank-one and similarity constraints and find an approximate solution to (29). Finally, we summarize the sequential optimization algorithm as follows.

Sequential Optimization Algorithm 2:

Input: $\{\theta_0, \theta_1, \ldots, \theta_K\}$, $\{\alpha_0, \alpha_1, \ldots, \alpha_K\}$, $\boldsymbol{s}_0$
Output: A solution $(\boldsymbol{s}^\star, \boldsymbol{w}^\star)$ of (16).

1) For $m = 1$, initialize $\boldsymbol{s}_1 = \boldsymbol{s}_0$, and compute $\boldsymbol{w}_1$ as

$$\boldsymbol{w}_1 = \frac{[\mathbf{\Sigma}_I(\boldsymbol{s}_1) + \mathbf{I}]^{-1}\mathbf{A}(\theta_0)\boldsymbol{s}_1}{\boldsymbol{s}_1^\dagger \mathbf{A}^\dagger(\theta_0)[\mathbf{\Sigma}_I(\boldsymbol{s}_1) + \mathbf{I}]^{-1}\mathbf{A}(\theta_0)\boldsymbol{s}_1},$$

where $\mathbf{\Sigma}_I(\boldsymbol{s}_1) = \sum_{k=1}^K \mathrm{INR}_k \mathbf{A}(\theta_k)\boldsymbol{s}_1\boldsymbol{s}_1^\dagger \mathbf{A}^\dagger(\theta_k)$, and $\mathrm{INR}_k = E[|\alpha_k|^2]/\sigma_v^2$, $k = 1, \ldots, K$. Then, the initialization SINR can be calculated as $\mathrm{SINR}_1 = \rho(\boldsymbol{s}_1, \boldsymbol{w}_1)$. The computational complexity in this step is about $\mathcal{O}(N^3 N_T^3)$ flops [29].

- Let $m = m + 1$, run the SDR and randomization steps as follows.
- Compute $\mathbf{\Sigma}_t(\boldsymbol{w}_{m-1})$ and $\mathbf{\Phi}(\boldsymbol{w}_{m-1})$ as

$$\mathbf{\Sigma}_t(\boldsymbol{w}_{m-1}) = \mathbf{A}^\dagger(\theta_0)\boldsymbol{w}_{m-1}\boldsymbol{w}_{m-1}^\dagger \mathbf{A}(\theta_0),$$
$$\mathbf{\Phi}(\boldsymbol{w}_{m-1}) = \mathbf{\Sigma}_I(\boldsymbol{w}_{m-1}) + \boldsymbol{w}_{m-1}^\dagger \boldsymbol{w}_{m-1}\mathbf{I},$$

where

$$\mathbf{\Sigma}_I(\boldsymbol{w}_{m-1}) = \sum_{k=1}^K \mathrm{INR}_k \mathbf{A}^\dagger(\theta_k)\boldsymbol{w}_{m-1}\boldsymbol{w}_{m-1}^\dagger \mathbf{A}(\theta_k).$$

The computational complexity is in the order of $\mathcal{O}(N^2 N_T^2)$ flops.

- SDP: Solve the SDP problem below and denote by $(\mathbf{X}^\star, y^\star)$ a solution

$$\begin{aligned} \text{(SDP)} \max_{\mathbf{X},y} \quad & \mathrm{tr}\left[\mathbf{\Sigma}_t(\boldsymbol{w}_{m-1})\mathbf{X}\right], \\ \text{s.t.} \quad & \mathrm{tr}[\mathbf{\Phi}(\boldsymbol{w}_{m-1})\mathbf{X}] = 1 \\ & \mathrm{diag}(\mathbf{X}) = y\mathbf{I} \\ & \mathbf{X} \succeq 0, y \geq 0, \end{aligned} \tag{32}$$

which requires about $\mathcal{O}(N^{3.5} N_T^{3.5})$ flops [26].

- Randomization: Let $\mathbf{Z}^\star = \mathbf{X}^\star / y^\star$, and generate random vectors $\boldsymbol{\xi}_i \in C^{N_T N \times 1}$, $i = 1, \ldots, L$, where L is the number of randomization trials, from a circular complex Gaussian distribution with zero mean and covariance

$$\mathbf{C} = \mathbf{Z}^\star \odot \boldsymbol{p}_c \boldsymbol{p}_c^\dagger.$$

For the ith randomization trial, let $\boldsymbol{s}_{m,i}(k) = \boldsymbol{p}_c^*(k)\mu(\boldsymbol{\xi}_i(k))$, $k = 1, \ldots, N_T N$, where

$$\mu(\boldsymbol{\xi}_i(k)) = \exp\left(j\frac{\arg(\boldsymbol{\xi}_i(k))}{2\pi}\delta_k\right).$$

Choose $\boldsymbol{s}_m$ from $\boldsymbol{s}_{m,i}$, such that

$$\boldsymbol{s}_m = \arg\max_{\boldsymbol{s}_{m,i}} \frac{\boldsymbol{s}_{m,i}^\dagger \mathbf{\Sigma}_t(\boldsymbol{w}_{m-1})\boldsymbol{s}_{m,i}}{\boldsymbol{s}_{m,i}^\dagger \mathbf{\Phi}(\boldsymbol{w}_{m-1})\boldsymbol{s}_{m,i}}.$$

The computational complexity in this step for L randomizations is $\mathcal{O}(LN^2 N_T^2)$ flops [26].

- Compute $\boldsymbol{w}_m$ as

$$\boldsymbol{w}_m = \frac{[\mathbf{\Sigma}_I(\boldsymbol{s}_m) + \mathbf{I}]^{-1}\mathbf{A}(\theta_0)\boldsymbol{s}_m}{\boldsymbol{s}_m^\dagger \mathbf{A}^\dagger(\theta_0)[\mathbf{\Sigma}_I(\boldsymbol{s}_m) + \mathbf{I}]^{-1}\mathbf{A}(\theta_0)\boldsymbol{s}_m},$$

where

$$\mathbf{\Sigma}_I(\boldsymbol{s}_m) = \sum_{k=1}^K \mathrm{INR}_k \mathbf{A}(\theta_k)\boldsymbol{s}_m\boldsymbol{s}_m^\dagger \mathbf{A}^\dagger(\theta_k),$$

which has the computational complexity of $\mathcal{O}(N^3 N_T^3)$ flops [29].

- The SINR at the mth iteration can be calculated as

$$\mathrm{SINR}_m = \rho(\boldsymbol{s}_m, \boldsymbol{w}_m).$$

If $|\mathrm{SINR}_m - \mathrm{SINR}_{m-1}| \leq \varepsilon$, where ϵ is a user selected parameter to control convergence, output $\boldsymbol{s}^\star = \boldsymbol{s}_m$ and $\boldsymbol{w}^\star = \boldsymbol{w}_m$; otherwise, repeat step 2) until convergence. The computational complexity is in the order of $\mathcal{O}(N^2 N_T^2)$ flops [29].

To summarize, the overall computational complexity of Algorithm 2 is in order of $\mathcal{O}(PN^{3.5}N_T^{3.5}) + \mathcal{O}(PLN^2 N_T^2)$, again mainly due to SDP and randomization. While this expression is the same as that for Algorithm 1, numerical simulations (see Section V) show that Algorithm 2 takes longer time to converge ($P \approx 30$) but requires fewer randomization trials ($L \approx 200$) than Algorithm 1.

V. Numerical Results

We evaluate the proposed waveform design algorithms via numerical simulations. We assume that both the transmitter and receiver are ULAs of respectively $N_T = 4$ and $N_R = 8$ elements with half-wavelength inter-element separation. A target is located at the spatial angle θ_0 with power $|\alpha_0|^2 = 20$ dB; and three fixed interferences are located at the spatial angles $\theta_1 = -50°$, $\theta_2 = -10°$, and $\theta_3 = 40°$, respectively. The power for each interference is $|\alpha_i|^2 = 30$ dB, $i = 1, 2, 3$. The noise

variance is $\sigma_v^2 = 0$ dB. We consider the orthogonal linear frequency modulation (LFM) as the reference waveform. Denote by $\mathbf{S}_0$ the space-time waveform matrix of the LFM waveform. The (k,n)th entry of $\mathbf{S}_0$ is

$$\mathbf{S}_0(k,n) = \frac{\exp\{j2\pi k(n-1)/N\}\exp\{j\pi(n-1)^2/N\}}{\sqrt{NN_T}}, \tag{33}$$

where $k = 1,\ldots,N_T$ and $n = 1,\ldots,N$. The $N_T N \times 1$ vector $\boldsymbol{s}_0$ is obtained by stacking the columns of $\mathbf{S}_0$. Notice that LFM waveforms have good properties in the pulse compression and ambiguity, and they are good candidates for distinguishing point targets and imaging [30]. However, it may not have good SINR performance in a clutter environment.

In the sequel, we use **SOA1-CMC** and **SOA2-CMC** to denote respectively the proposed Sequential Optimization Algorithms 1 and 2 with Constant Modulus Constraint, **SOA1-CMSC** and **SOA2-CMSC** to denote respectively the proposed Sequential Optimization Algorithms 1 and 2 with Constant Modulus and Similarity Constraints. Moreover, the algorithms provided in [16] and [18] are respectively denoted by **SOA1-EC** and **SOA2-EC** (Sequential Optimization Algorithms 1 and 2 with Energy Constraint). In our simulations, the number of randomization trials for SOA1 is $L = 20000$, while for SOA2 it is $L = 200$. We found it is necessary to use more trials for SOA1 to reach a good performance. The initialization waveform for both algorithms is $\boldsymbol{s}_0$, when the similarity constraint is or is not imposed.

A. Waveforms With Constant Modulus Constraint

In this subsection, we consider waveforms obtained from the proposed algorithms with only constant modulus constraint (i.e., SOA1-CMC and SOA2-CMC), which is equivalent to setting the similarity parameter $\epsilon = 2$. For comparison, the algorithms subject to the energy constraint (i.e., SOA1-EC and SOA2-EC) are also evaluated. In addition, we assess the interference suppression capability of these waveforms through the beampattern $P(\theta)$. Specifically, denote by $\boldsymbol{s}^\star$ and $\boldsymbol{w}^\star$ the optimal waveform and receive filter. Then the beampattern $P(\theta)$ can be computed as

$$P(\theta) = \left|(\boldsymbol{w}^\star)^\dagger \mathbf{A}(\theta)\boldsymbol{s}^\star\right|^2, \tag{34}$$

where $\mathbf{A}(\theta)$ is given in (6).

Figs. 1 and 2 depicts the SINR behaviors and beampatterns for two different target location θ_0. Inspection on SINR behavior for $\theta_0 = 15°$ in Fig. 1 (left plot) reveals that the SINR values of the SOA1-CMC and SOA1-EC increase with the iteration number, and both are converge very fast (i.e., after 2–3 iterations). As for the SOA2-EC and SOA2-CMC, the convergence speed is slower (i.e., need about 30 iterations). It is interesting to note that the optimal SINR values for the four algorithms are nearly the same and, therefore, there is no significant loss of SINR by imposing the constant modulus constraint. This clearly motivates adding this constraint in MIMO waveform design, since it is favored by efficient nonlinear power amplifiers. Compared with the upper bound of the SINR $= 20$ dB, which is attained when the interferences are absent or fully suppressed, the performance gap is less than 0.3 dB. This is because the target and interferences are widely separated in current case, resulting in good interference suppression performance. The beampatterns in Fig. 1 (right plot) show the nulls are clearly placed at the locations of interferences and the levels of the nulls are about -90 dB.

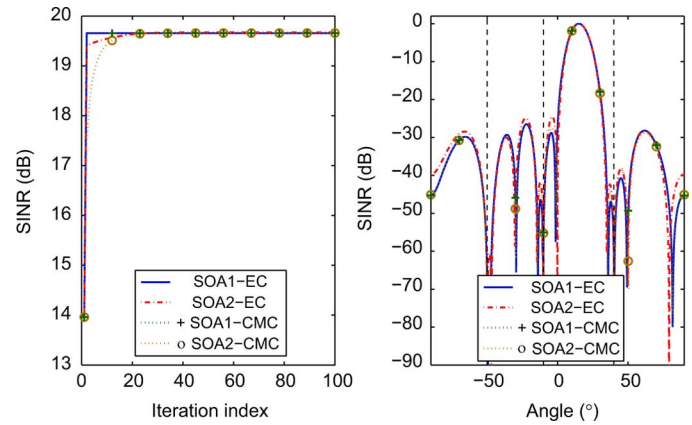

Fig. 1. The SINR (left plot) and beampattern $P(\theta)$ (right plot) with constant modulus constraint. Target location: $\theta_0 = 15°$. Other parameters: $N_T = 4$, $N_R = 8$, $N = 16$, $L_0 = 100$, $\epsilon = 2$, $\theta_0 = 15°$, $\theta_1 = -50°$, $\theta_2 = -10°$, $\theta_3 = 40°$, $|\alpha_0|^2 = 20$ dB, $|\alpha_v|^2 = 0$ dB, and $|\alpha_1|^2 = |\alpha_2|^2 = |\alpha_3|^2 = 30$ dB.

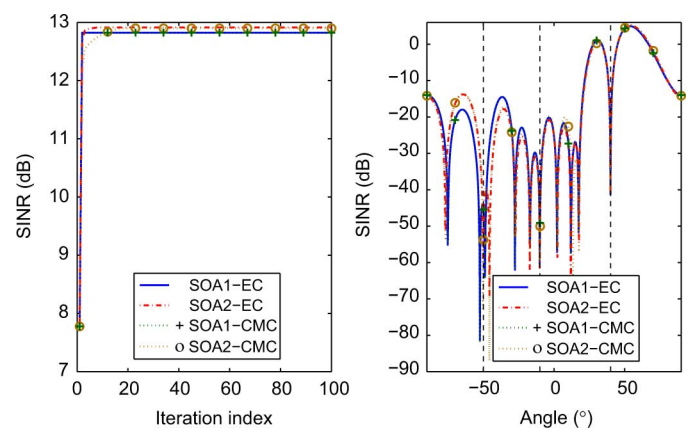

Fig. 2. The SINR (left plot) and beampattern $P(\theta)$ (right plot) with constant modulus constraint. Target location: $\theta_0 = 45°$. Other parameters: same as in Fig. 1.

The SINR behaviors decreases as the target is close to some interference source. In Fig. 2, the target is located at $\theta_0 = 45°$ which is close to interference $\theta_3 = 40°$. In this case, the gap between the SINR of any of the 4 algorithms and the SINR upperbound is enlarged to about 7 dB (cf., it was about 0.3 dB in Fig. 1). Moreover, the optimal SINR values of the SOA2-EC and SOA2-CMC are slight better than that of the SOA1-EC and SOA1-CMC. The beampatterns in Fig. 2 also show the null located at θ_3 is not as deep as the nulls at the other two interference locations. Interestingly, like in Fig. 1, there is no loss of imposing the constant modulus constraint for both the SOA1 and SOA2 algorithms.

B. Waveforms for Both Constant Modulus and Similarity Constraints

In this subsection, we consider waveforms designed by the proposed algorithms with both constant modulus and similarity constraints. Specifically, we evaluate the performances of the

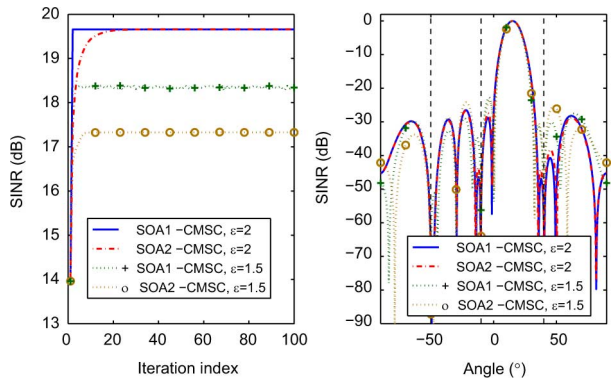

Fig. 3. The SINR (left plot) and beampattern $P(\theta)$ (right plot) with constant modulus and similarity constraints. Similarity parameter: $\epsilon = 1.5$ and 2. Other parameters: same as in Fig. 1.

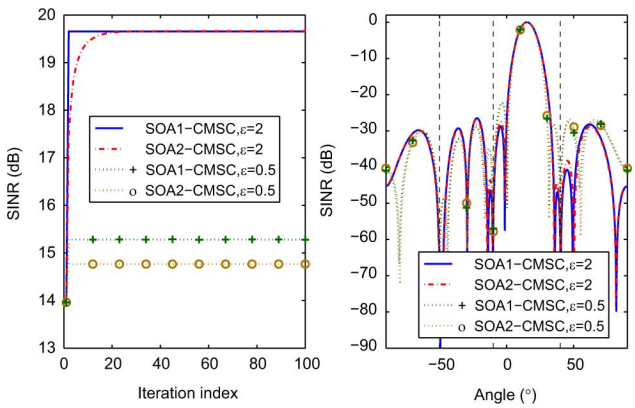

Fig. 4. The SINR (left plot) and beampattern $P(\theta)$ (right plot) with constant modulus and similarity constraint. Similarity: $\epsilon = 0.5$ and 2. Other parameters: same as in Fig. 1.

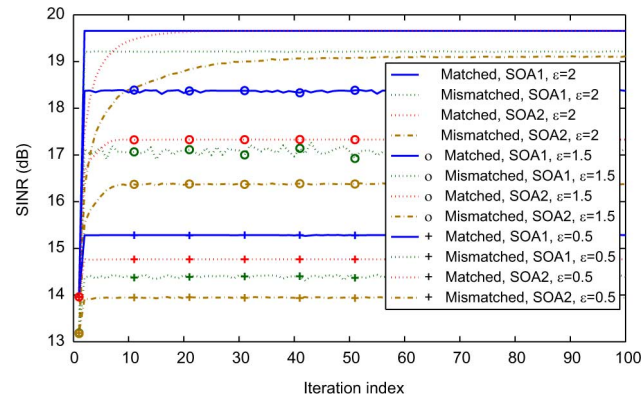

Fig. 5. The SINR with knowledge of the exact locations *(matched)* and mean locations *(mismatched)* of the interferences. Similarity: $\epsilon = 2, 1.5$ and 0.5.

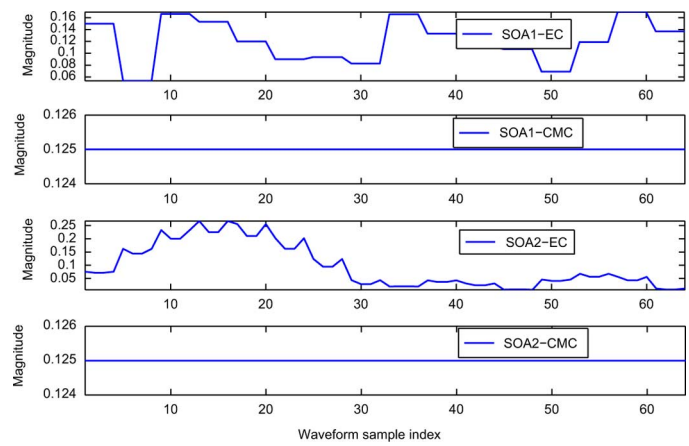

Fig. 6. The amplitude of designed waveforms with and without the constant modulus constraint.

SOA1-CMSC and SOA2-CMSC with two different levels of similarity, namely $\epsilon = 1.5$ and $\epsilon = 0.5$, where we recall $0 \leq \epsilon \leq 2$ defined in (11) controls the level of similarity, with $\epsilon = 2$ corresponding to the case of no similarity constraint and $\epsilon = 0$ to the case of full similarity (i.e., the designed waveform is identical to the reference waveform). The results are shown in Fig. 3 for $\epsilon = 1.5$ and Fig. 4 for $\epsilon = 0.5$. In both figures, we also include the results with $\epsilon = 2$ for comparison. It is clearly seen that the similarity constraint incurs an SINR loss. For example, with $\epsilon = 1.5$, the loss for SOA1-CMSC and SOA2-CMSC is 1.3 dB and, respectively, 2.4 dB. In general, the smaller the value of ϵ, the higher the SINR loss. We also observed that (not shown here) the SINR loss tends to a fixed value as ϵ approaches 0, in which case the designed waveform becomes identical to the reference LFM chirp waveform and the SINR loss is essentially that of the LFM. The beampatterns show that as the similarity constraint becomes stronger, the interference null also becomes higher. For example, we see the nulls are respectively -85 dB, -65 dB, and -63 dB for $\theta_1 = -50°$, $\theta_2 = -10°$, and $\theta_3 = 40°$; and they become about -75 dB, -58 dB, and -59 dB for $\epsilon = 0.5$.

Unlike the previous numerical simulations which assumes exact knowledge of the interferer angles, we consider here a mismatched case when the locations are random variables and only their mean is given. Specifically, the locations of the 3 interferers are modeled as Gaussian random variables with statistical mean given by $\theta_1 = -50°$, $\theta_2 = -10°$, and $\theta_3 = 40°$, respectively, and the variance $\sigma^2 = 4°$. Fig. 5 shows the SINR obtained by the SOA1 and SOA2 with different levels of similarity as considered in Figs. 3 and 4. Both the *matched* case (i.e., the exact interference locations are known) and *mismatched* case (only the mean locations are known) are considered. The curves demonstrate that both SOA1 and SOA2 exhibit a SINR loss for the mismatched case for all ϵ compared with matched case. For example, the SINR losses of the SOA1 between matched and mismatched angles are respectively about 0.5 dB for $\epsilon = 2$, 1.4 dB for $\epsilon = 1.5$, and 0.9 dB for $\epsilon = 0.5$. For the SOA2, they are about 0.55 dB, 0.9 dB, and 0.9 dB, respectively.

C. Waveform Properties and Pulse Compression

Waveform Properties in terms of the amplitude, phase and pulse compression are examined in this subsection. Fig. 6 depicts the magnitude of the $N_T N \times 1$ waveform vector $\boldsymbol{s}^\star$ obtained respectively by the SOA1-EC, SOA1-CMC, SOA2-EC, and SOA2-CMC with $\epsilon = 2$ (no similarity constraint), where the other parameters are similar to those in Fig. 1. The results show that for the SOA1-EC and SOA2-EC, the amplitude fluctuates are fluctuating both in the temporal and spatial domains. The fluctuations range from 0.055 to 0.17 for the SOA1-EC, and from 0.01 to 0.27 for the SOA2-EC. By considering the constant modulus constraint in the optimization procedure, the amplitude of the waveform obtained by SOA1-CMC or SOA2-CMC is constant.

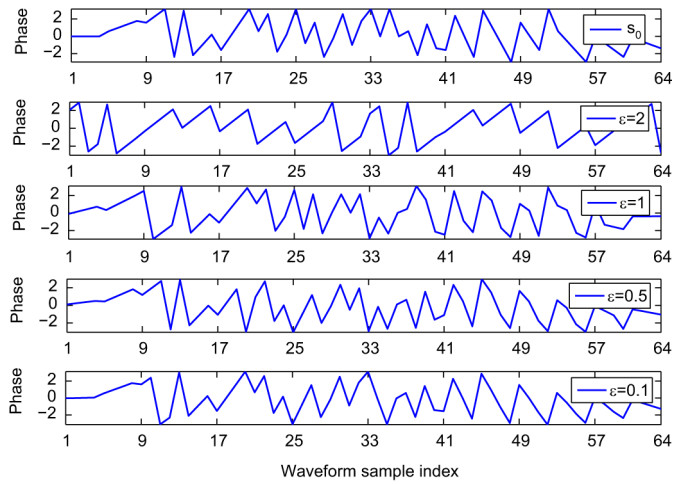

(a)

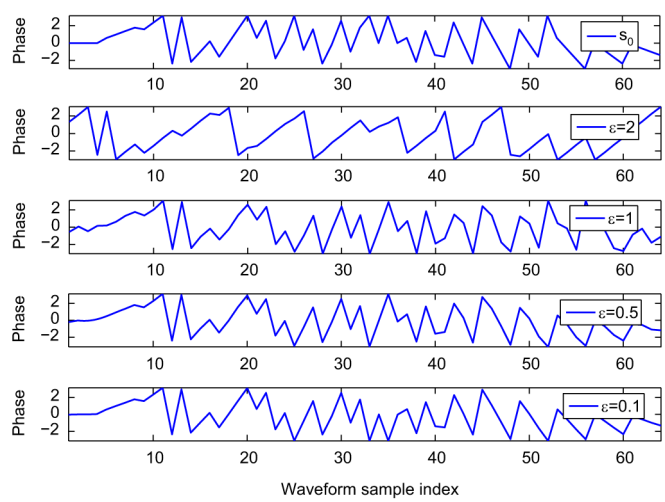

(b)

Fig. 7. The phase of the waveforms obtained by (a) the SOA1-CMSC and (b) the SOA2-CMSC with the constant modulus constraint and several levels (ϵ) of the similarity constraint.

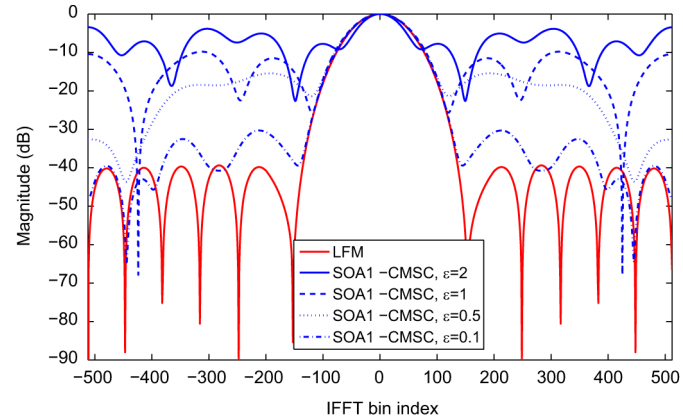

(a)

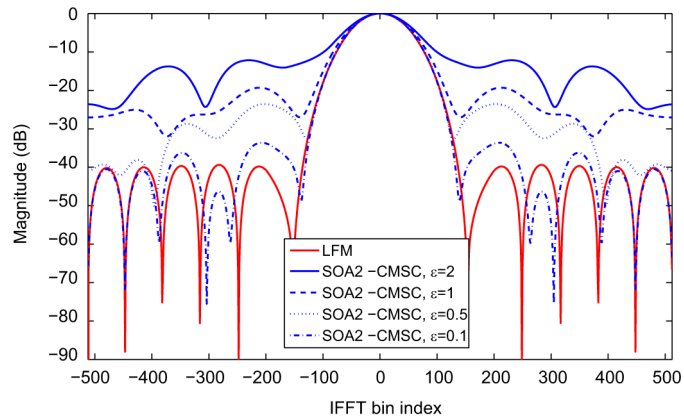

(b)

Fig. 8. Pulse compression profile of the waveform obtained by (a) the SOA1-CMSC and (b) the SOA2-CMSC with the constant modulus constraint and several levels (ϵ) of the similarity constraint.

Next, we consider the phase properties of the waveforms obtained with the similarity constraint. Figs. 7(a) and 7(b) show the phase of the waveforms obtained by the SOA1-CMSC and SOA2-CMSC, respectively, where several levels of similarity ϵ is considered. The simulation parameters are similar to those in Fig. 3. For comparison, the phase of the reference LFM waveform is also included to check the similarity of the designed waveforms. The amplitude of all waveforms is constant and, therefore, not shown here. It is seen from the figures that as ϵ decreases, the waveforms obtained by both algorithms become more and more similar to the LFM. This behavior agrees with the fact that the smaller the value of ϵ, the stronger the phase constraint on the designed waveforms.

Finally, we consider the pulse compression property of the designed waveforms. To this end, we reshape the $N_T N \times 1$ vector $\boldsymbol{s}^\star$ obtained by either the SOA1-CMSC or SOA2-CMSC to a new $N_T \times N$ matrix $\mathbf{S}^\star$, so that each row of $\mathbf{S}^\star$ contains the samples of the waveform emitted from one transmit element. Let $\boldsymbol{s}_n^\star$ denote the nth row of matrix $\mathbf{S}^\star$, $n = 1, \ldots, N_T$. In the following, we use $\boldsymbol{s}_1^\star$, while the results are similar with other rows of $S^\star$. We use the matched filter implemented in the frequency domain to obtain the range profile [30]. Specifically, we use the following procedure:

1) First, compute the Fast Fourier Transform (FFT) of $s_1^\star$: $\boldsymbol{f} = \mathrm{FFT}(\boldsymbol{s}_1^\star)$;
2) Second, multiply $\boldsymbol{f}$ by its conjugate $\boldsymbol{f}^*$, along with a hamming widow $\boldsymbol{h}$ with length N to suppress the sidelobe levels, i.e., $\boldsymbol{f}_p = \boldsymbol{f}\boldsymbol{f}^*\boldsymbol{h}$;
3) Finally, transform $\boldsymbol{f}_p$ to the time domain by the inverse Fast Fourier Transform (IFFT), i.e., $\boldsymbol{r}_p = \mathrm{IFFT}(\boldsymbol{f}_p, N_f)$, where N_f is the IFFT points.

Figs. 8(a) and 8(b) show the range profile $\boldsymbol{r}_p$ obtained by the SOA1-CMSC and SOA2-CMSC, respectively, where similarity parameter ϵ are considered and the other simulation parameters are similar to those in Fig. 3. For comparison, the range profile obtained by using the reference LFM waveform is also included. The results show that as ϵ increases, the side lobe level becomes higher and higher. Specifically, for $\epsilon = 2$, the side lobe level is nearly the same as the main lobe level; and they are respectively about -10 dB and -15 dB for $\epsilon = 1$ and $\epsilon = 0.5$. It is important to recall from previous simulation results a larger ϵ generally yields a higher output SINR. Hence, in practice, the choice of the similarity level ϵ should be made by an appropriate tradeoff between the range solution and output SINR of the resulting waveform.

VI. Conclusions

In this paper, we have addressed the problem of MIMO radar waveform design in an environment with signal-dependent interference plus noise. We consider a narrow band colocated MIMO radar involving a point like target and several interference sources separated in the spatial space. Summarizing:

- We have proposed two sequential optimization algorithms SOA1 and SOA2 by maximizing the receiver output SINR, accounting for the constant modulus constraint as well as a similarity constraint between the transmitted signal and a reference waveform. Since each iteration of the proposed algorithms requires solving a non-convex problem whose exact solution cannot be found, we have resorted to the SDR and randomization technique to obtain approximate solutions with good accuracy. The computational complexity is only linear in the numbers of iterations and the number of randomization trials, and polynomial in the receive filter length.
- We have assessed the performance of the proposed optimization algorithms through numerical simulations. The results indicate that the constant envelope constraint leads to waveforms with little SINR loss compared with those obtained without the constraint. This clearly motivates the use of our constant modulus waveforms which can be used with efficient nonlinear power amplifiers. We also observed that the larger the similarity parameter ϵ (i.e., the weaker the similarity constraint), the larger the output SINR, but the poorer the pulse compression performance. This suggests a suitable tradeoff between the target detection probability and the range resolution should be considered in practice. Moreover, the SINR behaviors of the two algorithms indicate that the optimal SINR values of the SOA1 and SOA2 are nearly the same for widely separated target and interferences, but it is better for the SOA2 when target is close to the interference sources. Finally, when only the approximate locations of the interferences are known, the proposed algorithms exhibit some SINR loss.

A possible future work might concern the study of the multiple target situation [14] as well as adaptive waveform design [17] subject to necessary constraints (i.e., constant modulus, peak-average-ratio (PAR), and similarity). Finally, it might be of interest to extend the framework to MIMO ambiguity function shaping [31].

References

[1] J. Li and P. Stoica, *MIMO Radar Signal Processing*. Hoboken, NJ, USA: Wiley, 2009.

[2] E. Fishler, A. M. Haimovich, R. S. Blum, L. J. Cimini, Jr, D. Chizhik, and R. A. Valenzuela, "Spatial diversity in radars—models and detection performance," *IEEE Trans. Signal Process.*, vol. 54, no. 3, pp. 823–838, Mar. 2006.

[3] A. M. Haimovich, R. S. Blum, and L. J. Cimini, "MIMO radar with widely separated antennas," *IEEE Signal Process. Mag.*, vol. 25, no. 1, pp. 116–129, Jan. 2008.

[4] K. Forsythe, D. Bliss, and G. Fawcett, "Multiple-input multiple-output (MIMO) radar: Performance issues," in *Proc. 38th Asilomar Conf. Signals, Syst., Comput.*, Pacific Grove, CA, USA, Nov. 2004, vol. 1, pp. 310–315.

[5] J. Li and P. Stoica, "MIMO radar with colocated antennas," *IEEE Signal Process. Mag.*, vol. 24, no. 5, pp. 106–114, Sep. 2007.

[6] D. R. Fuhrmann and G. S. Antonio, "Transmit beamforming for MIMO radar systems using signal cross-correlation," *IEEE Trans. Aerosp. Electron. Syst.*, vol. 44, no. 1, pp. 171–186, Jan. 2008.

[7] P. Stoica, J. Li, and Y. Xie, "On probing signal design for MIMO radar," *IEEE Trans. Signal Process.*, vol. 55, no. 8, pp. 4151–4161, Aug. 2007.

[8] Y. Wang, X. Wang, H. Liu, and Z. Luo, "On the design of constant modulus probing signals for MIMO radar," *IEEE Trans. Signal Process.*, vol. 60, no. 8, pp. 4432–4438, Aug. 2012.

[9] G. S. Antonio, D. R. Fuhrmann, and F. C. Robey, "MIMO radar ambiguity functions," *IEEE J. Sel. Top. Signal Process.*, vol. 1, no. 1, pp. 167–177, Jan. 2007.

[10] C. Y. Chen and P. P. Vaidyanathan, "MIMO radar ambiguity properties and optimization using frequency-hopping waveforms," *IEEE Trans. Signal Process.*, vol. 56, no. 12, pp. 5926–5936, Dec. 2008.

[11] A. Aubry, M. Lops, A. M. Tulino, and L. Venturino, "On MIMO detection under non-Gaussian target scattering," *IEEE Trans. Inf. Theory*, vol. 56, no. 11, pp. 5822–5838, Nov. 2010.

[12] Y. Yang and R. S. Blum, "MIMO radar waveform design based on mutual information and minimum mean—square error estimation," *IEEE Trans. Aerosp. Electron. Syst.*, vol. 43, no. 1, pp. 330–343, Jan. 2007.

[13] Y. Yang and R. S. Blum, "Minimax robust MIMO radar waveform design," *IEEE J. Sel. Top. Signal Process.*, vol. 1, no. 1, pp. 147–155, Jun. 2007.

[14] A. Leshem, O. Naparstek, and A. Nehorai, "Information theoretic adaptive radar waveform design for multiple extended targets," *IEEE J. Sel. Top. Signal Process.*, vol. 1, no. 1, pp. 42–55, Jun. 2007.

[15] J. Li, L. Xu, P. Stoica, K. W. Forsythe, and D. Bliss, "Range compression and waveform optimization for MIMO radar: A Cramér-Rao bound based study," *IEEE Trans. Signal Process.*, vol. 56, no. 1, pp. 218–232, Jan. 2008.

[16] B. Friedlander, "Waveform design for MIMO radars," *IEEE Trans. Aerosp. Electron. Syst.*, vol. 43, no. 3, pp. 1227–1238, Jul. 2007.

[17] B. Friedlander, "On data—adaptive waveform design for MIMO radar," in *Proc. 41th Asilomar Conf. Signals, Syst., Comput.*, Pacific Grove, CA, USA, Nov. 2007, pp. 187–191.

[18] C. Y. Chen and P. P. Vaidyanathan, "MIMO radar waveform optimization with prior information of the extended target and clutter," *IEEE Trans. Signal Process.*, vol. 57, no. 9, pp. 3533–3544, Sep. 2009.

[19] T. Naghibi and F. Behnia, "MIMO radar waveform design in the presence of clutter," *IEEE Trans. Aerosp. Electron. Syst.*, vol. 47, no. 2, pp. 770–781, Apr. 2011.

[20] A. D. Maio, S. D. Nicola, Y. Huang, S. Zhang, and A. Farina, "Code design to optimize radar detection performance under accuracy and similarity constraints," *IEEE Trans. Signal Process.*, vol. 56, no. 11, pp. 5618–5629, Nov. 2008.

[21] A. D. Maio, S. D. Nicola, Y. Huang, Z. Luo, and S. Zhang, "Design of phase codes for radar performance optimization with a similarity constraint," *IEEE Trans. Signal Process.*, vol. 57, no. 2, pp. 610–621, Feb. 2009.

[22] A. D. Maio, Y. Huang, M. Piezzo, S. Zhang, and A. Farina, "Design of optimized radar codes with a peak to average power ratio constraint," *IEEE Trans. Signal Process.*, vol. 59, no. 6, pp. 2683–2697, Jun. 2010.

[23] S. Boyd and L. Vandenberghe, *Convex Optimization*. Cambridge, U.K.: Cambridge Univ. Press, 2004.

[24] J. Capon, "High resolution frequency-wavenumber spectrum analysis," *IEEE Proc.*, vol. 57, no. 8, pp. 1408–1418, Aug. 1969.

[25] Z. Luo, W. Ma, A. M. C. So, Y. Ye, and S. Zhang, "Semidefinite relaxation of quadratic optimization problems," *IEEE Signal Process. Mag.*, vol. 27, no. 3, pp. 20–34, May 2010.

[26] A. Aubry, A. D. Maio, M. Piezzo, A. Farina, and M. Wicks, "Cognitive design of the receive filter and transmitted phase code in reverberating environment," *IET Radar, Sonar, Navig.*, vol. 6, no. 9, pp. 822–833, Dec. 2012.

[27] A. Aubry, A. D. Maio, A. Farina, and M. Wicks, "Knowledge-aided (potentially cognitive) transmit signal and receive filter design in signal-dependent clutter," *IEEE Trans. Aerosp. Electron. Syst.*, vol. 49, no. 1, pp. 93–117, Jan. 2013.

[28] H. Li and B. Himed, "Transmit subaperturing for MIMO radars with co-located antennas," *IEEE J. Sel. Top. Signal Process.*, vol. 4, no. 1, pp. 55–65, Feb. 2010.

[29] G. H. Golub and C. F. Van Loan, *Matrix Computations*, 3rd ed. Baltimore, MD, USA: Johns Hopkins Univ. Press, 1996.

[30] M. A. Richards, J. A. Scheer, and W. A. Holm, *Principles of Modern Radar: Basic Principles*. New York, NY, USA: Scitech, 2010.

[31] A. Aubry, A. D. Maio, B. Jiang, and S. Zhang, "Ambiguity function shaping for cognitive radar via complex quartic optimization," *IEEE Trans. Signal Process.*, vol. 61, no. 22, pp. 5603–5619, Nov. 2013.

Guolong Cui (M'12) received the B.S., M.S., and Ph.D. degrees from University of Electronic Science and Technology of China (UESTC), Chengdu, in 2005, 2008, and 2012, respectively.

From January 2011 to April 2011, he was a visiting researcher with University of Naples Federico II, Naples, Italy. From June 2012 to August 2013, he was a postdoctoral researcher in the Department of Electrical and Computer Engineering, Stevens Institute of Technology, Hoboken, NJ. Since September 2013, he has been an Associate Professor in University of Electronic Science and Technology of China (UESTC). His current research interests include statistical signal processing in the field of statistical signal processing with emphasis on radars, waveform optimization, and passive sensing.

Hongbin Li (M'99–SM'08) received the B.S. and M.S. degrees from the University of Electronic Science and Technology of China, Chengdu, in 1991 and 1994, respectively, and the Ph.D. degree from the University of Florida, Gainesville, in 1999, all in electrical engineering.

From July 1996 to May 1999, he was a Research Assistant in the Department of Electrical and Computer Engineering, University of Florida. He was a Summer Visiting Faculty Member at the Air Force Research Laboratory in the summer of 2003, 2004, and 2009. Since July 1999, he has been with the Department of Electrical and Computer Engineering, Stevens Institute of Technology, Hoboken, NJ, where he is a Professor. His current research interests include statistical signal processing, wireless communications, and radars.

Dr. Li received the IEEE Jack Neubauer Memorial Award in 2013, the Outstanding Paper Award from the IEEE AFICON Conference in 2011, the Harvey N. Davis Teaching Award in 2003 and the Jess H. Davis Memorial Award for excellence in research in 2001 from Stevens Institute of Technology, and the Sigma Xi Graduate Research Award from the University of Florida in 1999. He is presently a member of the Signal Processing Theory and Methods (SPTM) Technical Committee and served on the Sensor Array and Multichannel (SAM) Technical Committee of the IEEE Signal Processing Society. He is an Associate Editor for EURASIP *Signal Processing*, and served on the editorial boards for the IEEE TRANSACTIONS ON WIRELESS COMMUNICATIONS, IEEE SIGNAL PROCESSING LETTERS, and the IEEE TRANSACTIONS ON SIGNAL PROCESSING. He was a Guest Editor for EURASIP *Journal on Applied Signal Processing* and a General Co-Chair for the 7th IEEE Sensor Array and Multichannel Signal Processing Workshop, Hoboken, NJ, June 17–20, 2012. He is a member of Tau Beta Pi and Phi Kappa Phi.

Muralidhar Rangaswamy (S'89–M'93–SM'98–F'06) received the B.E. degree in electronics engineering from Bangalore University, Bangalore, India, in 1985 and the M.S. and Ph.D. degrees in electrical engineering from Syracuse University, Syracuse, NY, in 1992.

He is presently with the Senior Advisor for Radar Research at the RF Exploitation Branch within the Sensors Directorate of the Air Force Research Laboratory (AFRL). Prior to this, he has held industrial and academic appointments. His research interests include radar signal processing, spectrum estimation, modeling non-Gaussian interference phenomena, and statistical communication theory. He has coauthored more than 150 refereed journal and conference record papers in the areas of his research interests. Additionally, he is a contributor to eight books and is a co-inventor on three U.S. patents.

Dr. Rangaswamy is the Technical Editor (Associate Editor-in-Chief) for Radar Systems in the IEEE TRANSACTIONS ON AEROSPACE AND ELECTRONIC SYSTEMS (IEEE-TAES). He served as the Co-Editor-in-Chief for the *Digital Signal Processing* journal between 2005 and 2011. He serves on the Senior Editorial Board of the IEEE JOURNAL OF SELECTED TOPICS IN SIGNAL PROCESSING (January 2012–December 2014). He was a 2–term elected member of the Sensor Array and Multichannel Processing Technical Committee (SAM-TC) of the IEEE Signal Processing Society between January 2005 and December 2010 and serves as a member of the Radar Systems Panel (RSP) in the IEEE-AES Society. He was the General Chairman for the 4th IEEE Workshop on Sensor Array and Multichannel Processing (SAM-2006), Waltham, MA, July 2006. He has served on the Technical Committee of the IEEE Radar Conference series in a myriad of roles (Track Chair, Session Chair, Special Session Organizer and Chair, Paper Selection Committee Member, Tutorial Lecturer). He served as the Publicity Chair for the First IEEE International Conference on Waveform Diversity and Design, Edinburgh, U.K. November 2004. He presently serves on the conference subcommittee of the RSP. He is the Technical Program Chairman for the 2014 IEEE Radar Conference. He received the 2012 IEEE Warren White Radar Award, the 2013 Affiliate Societies Council Dayton (ASC-D) Outstanding Scientist and Engineer Award, the 2007 IEEE Region 1 Award, the 2006 IEEE Boston Section Distinguished Member Award, and the 2005 IEEE-AESS Fred Nathanson Memorial Outstanding Young Radar Engineer award. He was elected as a Fellow of the IEEE in January 2006 with the citation "for contributions to mathematical techniques for radar space-time adaptive processing." He received the 2012 and 2005 Charles Ryan Basic Research award from the Sensors Directorate of AFRL, in addition to more than 40 scientific achievement awards.